AD-A163 015 ADHESION AND THE SURFACE BEHAVIOR OF THE SILICONE ELASTOMER RTV-142.. (U) AEROSPACE CORP EL SEGUNDO CA MATERIALS SCIENCES LAB R S BRETZLAFF ET AL. 01 NOV 85 1/1

UNCLASSIFIED TR-0086(6935-03)-1 SD-TR-85-79 F/G 11/10 NL

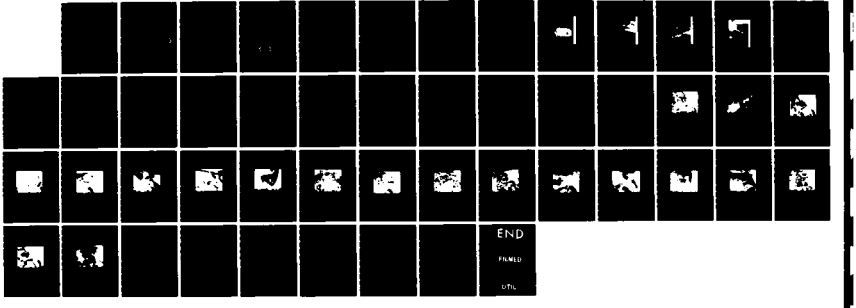

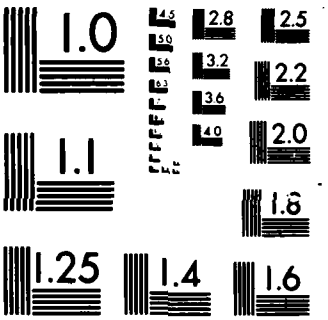

REPORT SD-TR-85-79

# Adhesion and the Surface Behavior of the Silicone Elastomer RTV-142

R. S. BRETZLAFF and T. A. FREITAG
Materials Sciences Laboratory
The Aerospace Corporation
El Segundo, CA 90245

and

A. Y. LEE
University of Illinois
Polymer Group
Urbana, IL 61801



1 November 1985





Prepared for

SPACE DIVISION
AIR FORCE SYSTEMS COMMAND
Los Angeles Air Force Station
P.O. Box 92960, Worldway Postal Center
Los Angeles, CA 90009-2960

This report was submitted by The Aerospace Corporation, El Segundo, CA 90245, under Contract No. F04701-85-C-0086 with the Space Division, P.O. Box 92960, Worldway Postal Center, Los Angeles, CA 90009-2960. It was reviewed and approved for The Aerospace Corporation by R. W. Fillers, Director, Materials Sciences Laboratory.

Capt David Thyfault SD/YNSA was the project officer for the Mission-Oriented Investigation and Experimentation (MOIE) Program.

This report has been reviewed by the Public Affairs Office (PAS) and is releasable to the National Technical Information Service (NTIS). At NTIS, it will be available to the general public, including foreign nationals.

This technical report has been reviewed and is approved for publication. Publication of this report does not constitute Air Force approval of the report's findings or conclusions. It is published only for the exchange and stimulation of ideas.

DAVID THYFAULT, Capt, USAF
MOIE Project Officer
SD/YNSA

JOSEPH HESS, GM-15
Director, AFSTC West Coast Office
AFSTC/WCO OL-AB

## PREFACE

The authors wish to thank A. Amram and J. Uht for the operation of the scanning electron microscope and B. Shenk for machining the sample substrates and curing the polymer. Calculation I was included after a helpful discussion with Professor R. Wool.

CONTENTS

## FIGURES

FIGURES (Continued)

# I. INTRODUCTION

The presence of small metal particles inside electronic circuit packages can cause short circuits. These particles are detected by the sound generated when they hit the package walls during a shaking procedure. This procedure is known as the Particle Impact Noise Detection, or PIND, test. The silicone elastomer RTV-142 is often applied to a portion of the inside wall area of the container to act as a particle getter, or "flypaper." Some examples of this adhesion are shown in Figures 1(a), 1(b), 2(a), and 2(b). It is desired to ascertain the mechanism of particle adhesion.

It is known theoretically that the presence of surfaces alters polymer chain statistics relative to their behavior in unbounded amorphous systems. For example, a crystallite surface affects nearly amorphous chains by offering the possibility for them to lower their free energy by recrystallizing. Furthermore, a Gaussian coil cannot exist near a free surface, because some of its segments would project beyond the surface, contrary to the definition of "free surface." An adjacent (e.g., metal) surface would allow surface chains the opportunity to lower their free energy by leaving their non-Gaussian conformation and moving onto the adjacent surface, interlocking with surface asperities and thereby causing adhesion. The apparent filleting shown in Figures 1(b), 2(a), and 2(b) seems to indicate that chains can rise above the surface to meet an adjacent particle. The indentation shown in Figures 2(a) and 2(b) seems to indicate that, as a fiber is incorporated into the surface, a depression of displaced chains may be left behind. Such large-scale chain mobility is only possible above $T_g$. For RTV-142, $T_g$ = -150°C as measured by differential scanning calorimetry.

Chain mobility can be demonstrated by taking scanning electron microscope (SEM) photos of surface features in RTV-142 as a function of temperature. If the chains are sufficiently mobile to obliterate surface features and move surface metal particles, then they should be sufficiently mobile to interlock with surface asperities of metal particles, causing adhesion.

Figure 1(a). SEM View of an RTV-142 Spot on the Inside Surface of an Electronics Package. A variety of metal filings has been collected during a PIND test.

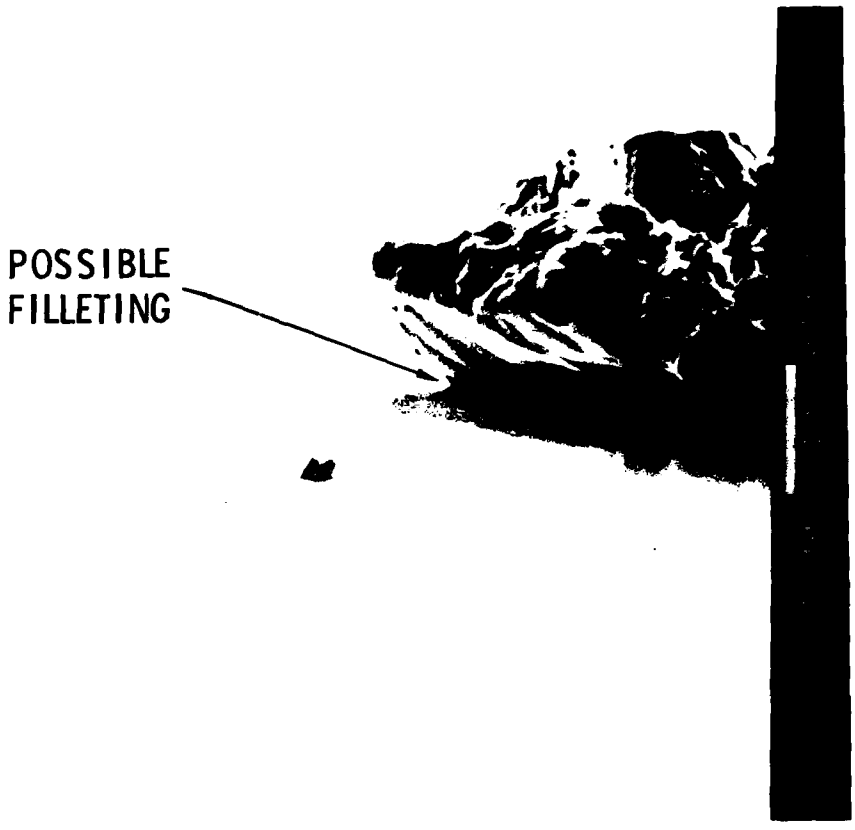


Figure 1(b). Enlarged View of a Metal Particle from Figure 1(a). Note the interfacial region which appears to be filleted.

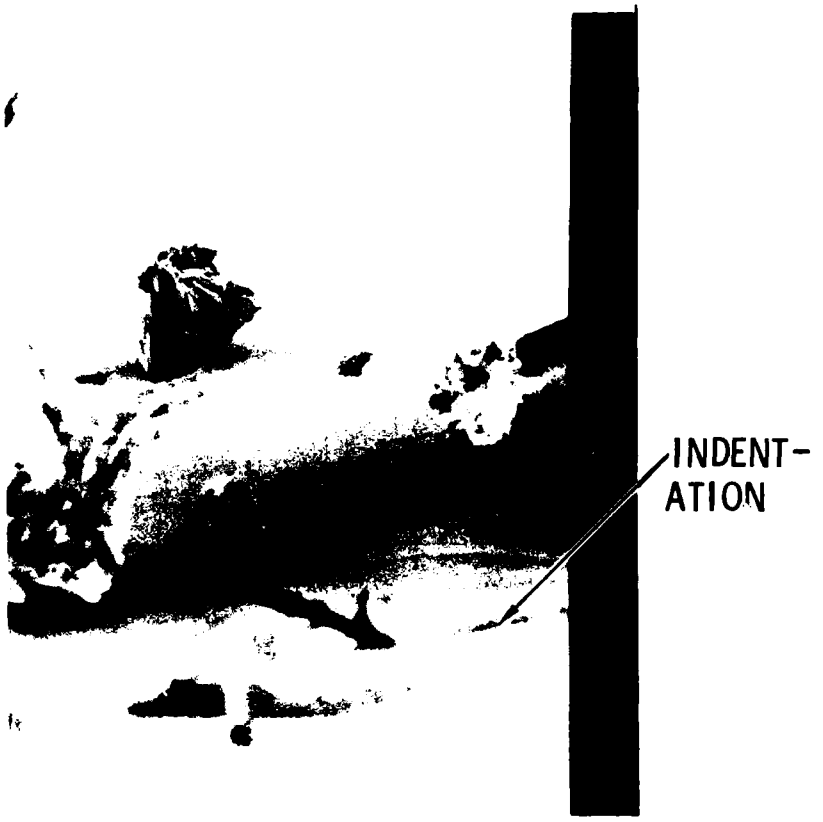


Figure 2(a). Grazing Angle View of the Surface Shown in Figure 1(a). Note the indentation near the fiber that enters the surface, as well as the possible filleting around the fiber

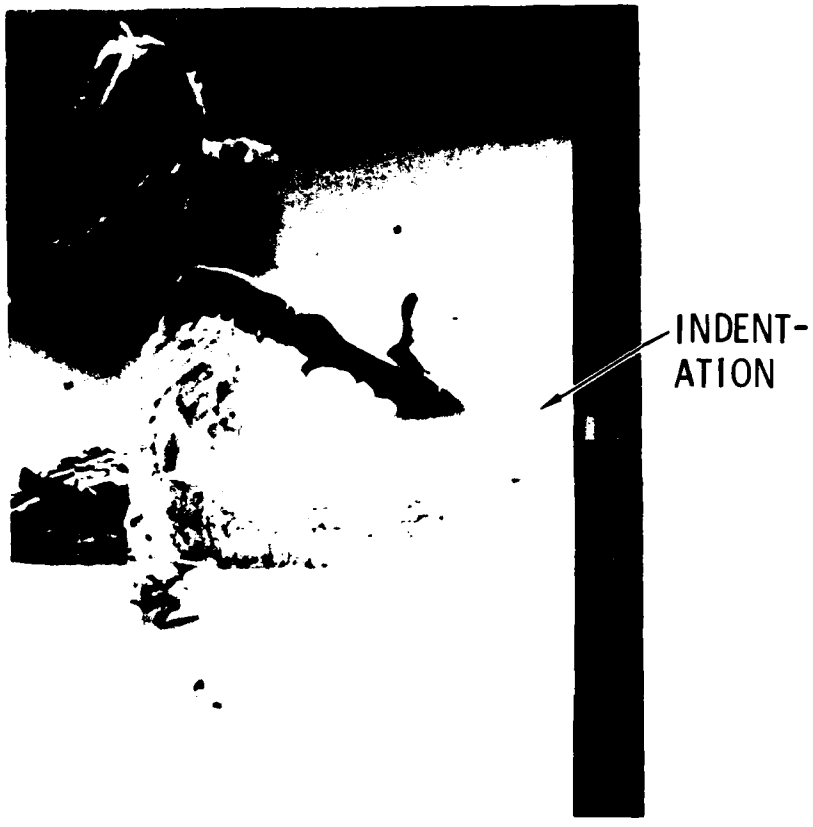


Figure 2(b). Enlarged View of the Fiber from Figure 2(a).

Another traditional school of thought in describing adhesion between macroscopic objects has considered forces acting at the molecular level. One of the first advances in this field was Van der Waals' explanation of real gas properties in terms of the interaction potential between two molecules.[1] The three effects considered were (i) interaction between permanent dipoles, (ii) the polarizing action of one molecule upon another, and (iii) a quantum mechanical attraction between non-polar atoms. The summation of the foregoing molecular forces is responsible for a number of colloidal phenomena.[2] Molecular forces parameters[3] appropriate for two parallel plates of polystyrene several angstroms apart can be shown to give an attractive energy per area of around 30 erg/cm$^2$. Molecular forces are responsible for bonding polyimide to a tungsten needlepoint in a field ion microscope study.[4] Thus, some polymers do exhibit molecular-force interactions to very smooth and clean surfaces. However, since there are many more chain segments than chain ends, and since the particles are rough and not necessarily very clean, we feel that surface rearrangement and mechanical interlocking may play a predominant role in the adhesion process.

Another author[5] believes that chemisorption (primary bonding of adhesive to substrate) is a major factor, because his experience with RTV silicones is that the presence of extractible silicones on the elastomer surface prevents adhesion without the use of a primer to overcome this potential weak boundary layer. However, our experience with RTV-142 and small metal particles is that effective adhesion does occur. This might be explained, on the chemisorption theory, by the possible absence of extractible silicones in RTV-142, or because a small weight-to-surface area ratio requires only a small adhesive strength. On the other hand, gold wire is also effectively "gettered" by the RTV-142, although it is difficult to form primary bonds to gold. Therefore we continue to look to surface chain mobility as the key to mechanical interlocking and adhesion.

## II. THEORETICAL

Packham[6] has noted that a liquid polymer will generally achieve good contact with a smooth, uncontaminated metal surface. While some studies have demonstrated worse adhesion on rougher surfaces, Packham points out that there are also well-established examples of anchor coats, into which polymer penetration is possible depending on the contact angle, $\theta$, the polymer surface energy, $\sigma$, and the shape of the pores. A polymer/anchor coat system shows increased adhesion, because fracture can no longer occur across a planar surface and because larger volumes of polymer may plastically deform to alter the stress distribution at the interface. Packham states that polymer surface energies are typically 50 to 100 erg/cm$^2$ and that the fractional penetration (i.e., the penetration depth of polymer into the pore divided by the total pore depth), $\xi$, into a cylindrical pore of radius, r, and filled with gas at pressure, p, is

$$\xi = \frac{w}{1 + w} \tag{1}$$

where $w = \sigma \cos \theta / pr \approx \sigma / pr$ ($\sigma$ is the surface tension). The bulk viscosity does not explicitly enter this surface analysis, although it may be implicitly related to $\sigma$ and $\theta$. If $\sigma = 10^2$ erg/cm$^2$ and $p = 10^6$ erg/cm$^3$, then $\xi = 99\%$ for $r = 100$ Å and $\xi = 0.1\%$ for $r = 1$ mm.

We wish to demonstrate that some idealized metal/solid-polymer surface energies can also be on the order of $10^2$ erg/cm$^2$. If this is true, then the idea of pore penetration and mechanical keying as the source of adhesion for metal particles is plausible. Metal particles having pores and irregularities on the 100 Å size scale would be suitable for about 99% penetration by the polymer chains in a $10^2$ erg/cm$^2$ surface-energy system. We will calculate the surface energy of an ideal polymer system in three ways, affording some complementary microscopic viewpoints of why there is an excess free energy at a free polymer surface compared to the free energy of an unbounded system. This will support the idea of an entropically driven flow of chain segments

into and around the metal particle asperities during the adhesion process. We consider only equilibrium processes; the kinetics of a particle approaching a surface at a finite speed are not considered, but the underlying effect would be the same.

One basic concept in this explanation is the idea of interpenetrating random-walk polymer chains in an unbounded polymer system. The surface energy is half the excess energy per unit area necessary to "cut" such a system with an infinite mathematical plane, creating two free surfaces. However, this "cut" is not allowed to break any primary bonds, because the free energy difference is evaluated at constant molecular weight. Therefore the presence of the mathematical plane must be considered as setting up a reflection boundary for the otherwise random-walking polymer chains. Each chain that intersects the plane is no longer a random-walk chain, but rather is constrained to turn around at the boundary and stay on one side or the other of the mathematical plane.

The first method of calculation was suggested by Professor Richard Wool.[7] The free energy increase per unit area is a simple counting procedure of the number of chains intersected by the plane for an unbounded system. This number per area is then multiplied by an estimate of the conformational energy necessary to "turn the chain around." This quantity is fairly well known from studies of the fold surfaces of polymer lamellae. In this view the energy to add enough gauche conformational states to bend the chain back on itself, rather than an entropic change, is responsible for the free energy increase. Since folding does involve an entropy change, it is not surprising that this first estimate is low.

The second calculation accounts for the entropy change caused by the presence of the free surface. In an unbounded polymer, random-walk statistics prescribes a Gaussian chain segment distribution function and an approximately spherical envelope within which a given percentage of a chain's segments is enclosed. If there are energetically distinct trans and gauche states, then the chain is not random-walk and has a more extended (ellipsoidal) envelope. A simple argument in statistical mechanics will be used to estimate how much

each original envelope is deformed by the presence of a free surface and what contribution this makes to the entropic term in the surface free energy.

The third calculation will employ the well known Green's Function technique for describing polymer chains. A system of random-walking chains in one dimension with and without the presence of a boundary will be analyzed and the entropy and free energy changes calculated. It will be seen that the entropic contribution to the free energy of an ideal system of amorphous chains gives an order of magnitude for the surface energy, $\sigma$, which makes plausible the entropically driven motion of polymer chain segments into metal particle asperities, reducing the excess free energy and causing adhesion.

CALCULATION I

Let $N_1$ be the number of chain intersections on a planar surface of area A. Let a be the chain cross-sectional area. Some chains intersect the plane obliquely. Therefore we take the typical effective chain area, $a_{eff}$, to be $a\sqrt{\langle\cos^2\beta\rangle}$, where $\beta$ is the angle between a chain axis and the normal to the cutting plane. The brackets denote averaging over all the chains. Supposing the polymer to be unoriented, with a Hermanns' orientation function $f = 0 = (3\langle\cos^2\beta\rangle-1)/2$, we have $\langle\cos^2\beta\rangle = \frac{1}{3}$ and $a_{eff} = \sqrt{3}a$ . (The average value of the function $\cos^2\beta$ is 1/2, but we find the argument from the Hermanns' orientation function more compelling.) Therefore,

$$N_1 = \frac{A}{\sqrt{3}a} \tag{2}$$

Considering a cylinder of basal area, a, and height, b, equal to the statistical monomer length, we can calculate the included chain mass as

$$ab\rho = ZM_o/N_a \tag{3}$$

where $\rho$ is the mass density, Z is the number of chemical repeat units in the statistical length, $M_o$ is the mass per mole of chemical repeating units, and $N_a$ is Avogadro's number. Hence,

$$\frac{N_i}{A} = \frac{b\rho N_a}{\sqrt{3}ZM_o} \tag{4}$$

Considering that no gauche conformations are necessary to turn around a chain with $\cos\beta = 0$ and that five or six gauches are necessary for a chain with $\cos\beta = 1$, we estimate that two extra gauche conformers are necessary on the average. (See Numerical Results I for more details of the conformational energy analysis.) Letting the conformational energy of the gauche state be $E_o$ above that of the trans state, we have

$$\sigma = \frac{N_i(2E_o)}{A} = \left[\frac{2}{\sqrt{3}}\left(\frac{b\rho N_a}{ZM_o}\right)\right] E_o \tag{5}$$

The factors in the square brackets in Eq. (5) define the number of extra gauche conformers per unit area, with $E_o$ being the energy per gauche conformer. Numerical results will be obtained below.

CALCULATION II

Consider a polymer layer of thickness, d, adjacent to a free surface. We will choose d to be equal to the radius of gyration of one polymer chain and consider all the coils within this "d-layer" to be uniformly deformed by the presence of the free surface. Outside the d-layer all the coils are assumed to be unaffected. We will estimate the coil deformation by noting that if two free surfaces were to be placed in contact and the coils were to interdiffuse to obliterate the boundary, each coil would have about twice as much volume available to it. From statistical mechanics,[8] then, we have

$$\Delta S = k \ln\left(\frac{\Omega'}{\Omega}\right) = k \ln\left(\frac{V'}{V}\right)^N \tag{6}$$

$$\Delta G = \Delta H - T\Delta S \tag{7}$$

where $\Delta S$, $\Delta G$, and $\Delta H$ are the changes in a coil's entropy, free energy, and enthalpy due to the presence of the free surface, $\Omega'$ ($\Omega$) are the numbers of configurations available to the coil in the deformed (undeformed) states, and $V'$ ($V$) are the volumes available to the coil in the deformed (undeformed) states. Considering only the entropic contribution ($\Delta H \approx 0$) and the previous assumption of volume-doubling for an undeformed compared to a deformed coil,

$$\Delta G_{coil} = -kT \ln\left(\frac{1}{2}\right)^N = NkT\ln 2 \tag{8}$$

The number, n, of affected coils in the depth, d, and under the area, A, is

$$n = \frac{dA\rho}{NZM_o/N_a} \tag{9}$$

Using $d = r_g = \sqrt{\frac{1}{6} Nb^2}$ in three dimensions, the total free energy change is

$$\Delta G_{tot} = \frac{dA\rho N_a}{NZM_o} \cdot NkT\ln 2 \tag{10}$$

whence

$$\sigma = \frac{\Delta G_{tot}}{A} = \left[\frac{\sqrt{N}}{\sqrt{6}} \left(\frac{b\rho N_a}{ZM_o}\right)\right] kT\ln 2 \tag{11}$$

The factors in the square brackets in Eq. (11) define the number of affected segments per unit area, with kTln2 being the extra energy per affected segment. Numerical results will be obtained below.

CALCULATION III

It is well known[9,10] that for a random-walk chain in one dimension,

$$G(x_1,x_2) = A \exp\left(\frac{-\Delta^2}{2Nb^2}\right) \tag{12}$$

where $\Delta = x_2 - x_1$; $x_2$ and $x_1$ are the coordinates of the chain ends; $G(x_1, x_2)$, the Green's function, is the number of configurations available to a chain of length Nb with ends at $x_1$ and $x_2$; and $\Lambda = (2\pi Nb^2)^{-1/2}$, with b having the same definition as above (statistical monomer length). Furthermore,

$$\Omega(x_1) = \int_{x_1-Nb}^{x_1+Nb} dx_2 G(x_1,x_2) \tag{13}$$

is the total number of configurations available to a chain with one end at $x_1$ and the other end unrestricted. A consequence of our definitions is that $\Omega(x_1)$ ranges from 0 to 1 as N ranges from 0 to infinity. Therefore, without loss of generality, our entropies vary from negative infinity to zero.

DiMarzio[9] has shown using the principle of images for a free surface that a chain will be "reflected" from every impingement on a free surface. The number, G′, of available configurations for the chain is thereby reduced. In fact,

$$G'(x_1,x_2) = \Lambda\left[\exp\left(\frac{-\Delta^2}{2Nb^2}\right) - \exp\left(\frac{-\sum^2}{2Nb^2}\right)\right] \tag{14}$$

where $\sum = x_2+x_1$. As previously,

$$\Omega'(x_1) = \int_{x_1-Nb}^{x_1+Nb} dx_2\ G'(x_1,x_2) \tag{15}$$

is the number of configurations available to a chain with one end at $x_1$ near a free surface. The integration limits in Eqs. (13) and (15) are the same, because the G′ expression accounts for the presence of the wall.

A straightforward mathematical analysis reveals that

$$\Omega(x_1) = \text{erf}\left(\sqrt{\frac{N}{2}}\right) \approx 1 - \frac{e^{-N/2}}{\sqrt{\pi N/2}} \tag{16}$$

for large N. Consequently,

$$S = k\ln\Omega \approx \frac{-ke^{-N/2}}{\sqrt{\pi N/2}} \approx 0 \tag{17}$$

For a deformed coil, Eqs. (14) and (15) yield

$$\Omega'(x_1) = \text{erf}\left(\sqrt{\frac{N}{2}}\right) - \frac{1}{2}\,\text{erf}\left(\sqrt{\frac{N}{2}}(1+\epsilon)\right) - \frac{1}{2}\,\text{erf}\left(\sqrt{\frac{N}{2}}(1-\epsilon)\right) \tag{18}$$

where $\epsilon = 2x_1/Nb$. Considering a chain with one end, $x_1$, close to the free surface compared to the chain length, Nb, but far away compared to one statistical monomer length, b, we have

$$b \ll 2x_1 \ll Nb \tag{19}$$

or

$$1 \ll N\epsilon \ll N \tag{20}$$

Under this assumption it follows that, for $\Delta H = 0$,

$$\Omega'(x_1) = \frac{e^{-N/2}}{\sqrt{2\pi N}}\,(1+\epsilon) \tag{21}$$

$$S' \approx -Nk/2 \tag{22}$$

$$\Delta G_{coil} \approx NkT/2 \tag{23}$$

The approximation in Eq. (19) or (20) is good for the entire d-layer (defined as in Calculation II) because $d = r_g = \sqrt{\frac{1}{2}Nb^2} << Nb$. Assuming as before that all the coils in the d-layer are similarly deformed, that the remaining coils are unaffected, and noting that this calculation is in one instead of three dimensions for simplicity, we have

$$\Delta G_{tot} = \frac{dA\rho N_a}{NzMo} (NkT/2) \tag{24}$$

whence

$$\sigma = \frac{\Delta G_{tot}}{A} = \left[\frac{\sqrt{N}}{\sqrt{2}} \left(\frac{b\rho N_a}{ZM_o}\right)\right] \frac{kT}{2} \tag{25}$$

One notes that this result is $\sqrt{3}/(2\ln 2)$, or 1.25, times larger than the result of Calculation II. Therefore the one-dimensional Green's function calculation describes about 25% more chain deformation, as measured by the surface energy, $\sigma$, than the simple volume-doubling calculation. Similarly, as in Eq. (11), the factors in the square brackets in Eq. (25) define the number of the affected segments per unit area, with kT/2 being the extra energy per affected segment. Numerical results are obtained below.

NUMERICAL RESULTS I

For a methyl siloxane chain we estimate b = 2 Si-O bond lengths ≈ 2 C-O bond lengths. Todokoro[11] has the C-O bond length as about 1.43 Å in PET. Hence we set b = 3.0 Å. Letting $M_o$ = 74 g/mole (Z=1), $\rho$ = 1.10 g/cm$^3$, and $N_a = 6.02 \times 10^{23}$ mole$^{-1}$, we obtain for the common factor in Eqs. (5), (11), and (25):

$$\frac{b\rho N_a}{ZM_o} = 0.268 \times 10^{15} \frac{\text{segments}}{\text{cm}^2} \tag{26}$$

A zeroth-order estimate of $E_o$ in Eq. (5) may be obtained from studies of the fold surface of polyethylene lamellae. This estimate is expected to have some relevance to siloxane chains: Although the methyl side groups are more restrictive to rotation, they are present only on alternating main-chain atoms, and, moreover, rotation around main-chain oxygens is relatively easy.

If the melting temperatures, Tm, of a series of specially-prepared polyethylene single crystals are graphed against the reciprocal lamellar thicknesses, $1/\ell$, the surface energy, $\sigma_e$, of the fold surface may be obtained as 93 ± 8 erg/cm$^2$.[12] For melt-crystallized material, $\sigma_e$ has been determined as 79.5 ± 2.5 erg/cm$^2$.[13] These results have been shown[14] to be consistent with a chain reversal at the fold surface achieved with 5 or 6 gauche conformers with $E_o$ = 0.8 kcal/mole = $0.522 \times 10^{-13}$ erg/gauche conformer. From Eqs. (5) and (26), we have

$$\sigma = \left(0.309 \times 10^{15} \frac{\text{gauche}}{\text{cm}^2}\right)\left(0.522 \times 10^{-13} \frac{\text{erg}}{\text{gauche}}\right) \tag{27a}$$

$$\sigma = 16.2 \text{ erg/cm}^2 \tag{27b}$$

This result, derived from conformational energy theory, is an order of magnitude less than the results derived from entropic considerations below. This indicates that the entropic effect is predominant for an idealized polymer system, subject to the validity of the $E_o$ estimate stated above.

NUMERICAL RESULTS II

From Eq. (11), the previous numerical assumptions, and the further assumptions of chain length $N = 10^4$ and of room temperature, it follows that

$$\sigma = \left(10.94 \times 10^{15} \frac{\text{segments}}{\text{cm}^2}\right)\left(0.0277 \times 10^{-12} \frac{\text{erg}}{\text{segment}}\right) \tag{28a}$$

$$\sigma = 303 \text{ erg/cm}^2 \tag{28b}$$

This theoretical result does not account for temperature-dependent chain stiffness or mobility. No enthalpic effects are included. In the ideal polymer system it is seen, however, that this calculation results in a surface-energy magnitude which, when used in Eq. (1), would predict chain segment flow into pores and around asperities of metal particles, consistent with adhesion.

NUMERICAL RESULTS III

Using Eq. (25) and the previous numerical assumptions, it follows that

$$\sigma = \left(18.95 \times 10^{15} \frac{\text{segments}}{\text{cm}^2}\right)\left(0.0200 \times 10^{-12} \frac{\text{erg}}{\text{segment}}\right) \tag{29a}$$

$$\sigma = 379 \text{ erg/cm}^2 \tag{29b}$$

As noted previously, this result is $\sqrt{3}/(2\ln 2)$ times larger than the estimate in Calculation II. It seems appropriate to state that the entropic contribution to the surface free energy of an ideal polymer system results in $\sigma \approx 300$ to 400 erg/cm$^2$, and that this contribution is more significant than the conformational fold-energy contribution, at around only 16 erg/cm$^2$, although this could change for hard-to-fold chains (high $E_o$).

In the 300-400 erg/cm$^2$ range, Eq. (1) prescribes a nearly 99% relative penetration of polymer into 100 Å pores or around asperities on the same size scale. Now we will turn to an experimental investigation of whether or not RTV-142 surfaces show motion that might be attributable to a flow of chain segments.

## III. EXPERIMENTAL RESULTS

A thin (few mils) layer of RTV-142 was cured for 24 hours on one face of a 3/8" diameter, 1/4" high Al cylinder. Then the layer was pressed between this cylinder and an identical one with a C-clamp for one week. The two cylinders were pulled apart just before cutting a pie shaped section on the elastomer surface, sprinkling some Al filings on that surface and mounting the supporting cylinder and elastomer surface on the cold stage of a JEOL JSM 35C scanning electron microscope. The stage thermocouple was mounted directly below the cylinder and registered -115°C within minutes of insertion. The quadrants of the surface under investigation are denoted by URQ, ULQ, LLQ, and LRQ for upper right, upper left, lower left, and lower right quadrants, respectively.

Figures 3-10 were obtained during the first 1-1/2 hours, during which time the sample temperature decreased to -135°C. Figures 11-12 were taken after 4 additional hours at -135°C. Then the stage was allowed to warm up overnight to room temperature. After a total of 18 hrs, Figures 13-17 were taken. The sample was then annealed at 100°C for 2 hours in an oven and reexamined in Figures 18-21 at room temperature. All results were obtained at 5 kV and magnification shown in each figure.

In interpreting these figures, it should be noted that there are competing effects: bulk thermal expansion, release of residual stresses from the fracture event, and surface chain mobility. Furthermore, the sample could not be carbon coated (in order to preserve surface chain mobility). Therefore, there is the possibility of beam-charging effects. Finally, one generally expects beam-damage effects to occur in polymeric systems.

In Figure 3, we see the URQ with the pie cut. The brighter regions are either the metal filings or polymer surfaces slightly raised by fracture or, in principle, by the reduction in temperature. Figure 3 designates metal particles P #1 and P #2, while metal particle P #3 (shown later) is just out of view, as indicated.

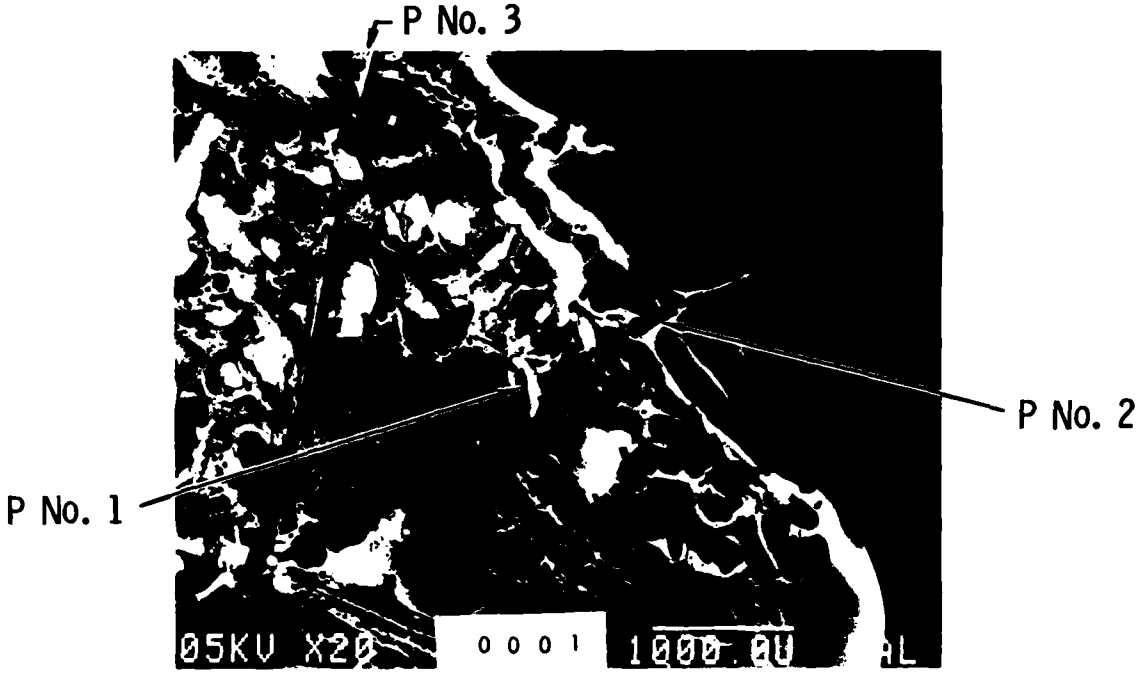


Figure 3. SEM View of the Upper Right Hand Quadrant (URQ) of the RTV-142 Surface Showing the Pie Cut and the Metal Particles. Particles P#1, P#2, and the general location of P#3 are noted. The beam voltage and magnification are noted in the lower left corner of all photos, and the scale marking is in the lower right corner. Low temperature and initial time intervals for Figures 3-10 (see text).


Figure 4. SEM View of Metal Particle P#1.


Figure 5. SEM View of Metal Particle P#2.

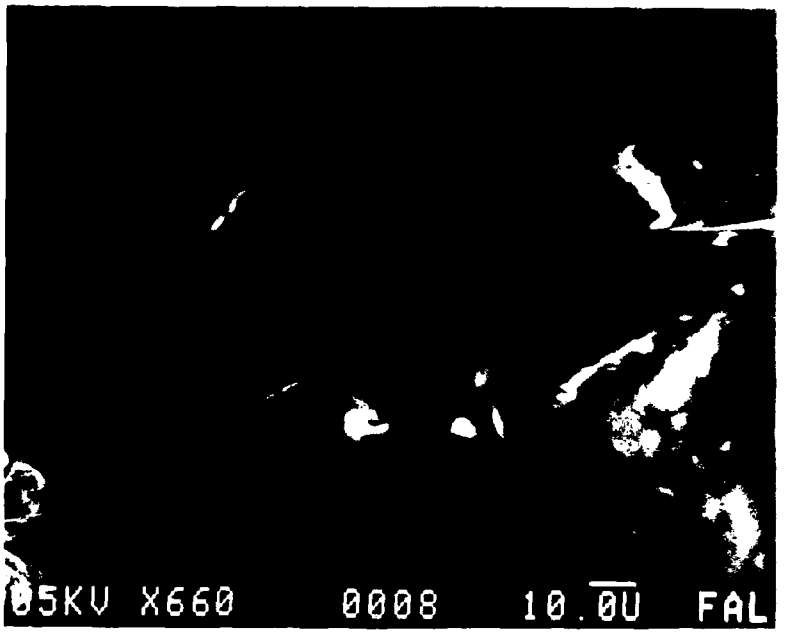


Figure 6. SEM View of Detail from Figure 5.


Figure 7. SEM View of Beam Damage Caused While Taking Photo for Figure 6.


Figure 8. First SEM View of a Long Fiber ($P^{\#}3$) in the General Location Noted in Figure 3.


Figure 9. Second SEM View of P#3.


Figure 10. SEM View of Detail in the Lower Right Hand Quadrant (LRQ) Including Beam Damage Rectangles.


Figure 11. URQ (compare Figure 3). Beam-damaged areas persist on the far right center because of electron intensity for previous photos. Low temperatures and 4 hours elapsed time for Figures 11 and 12 (see text).


Figure 12. Persistent Beam Damage from Figure 11.

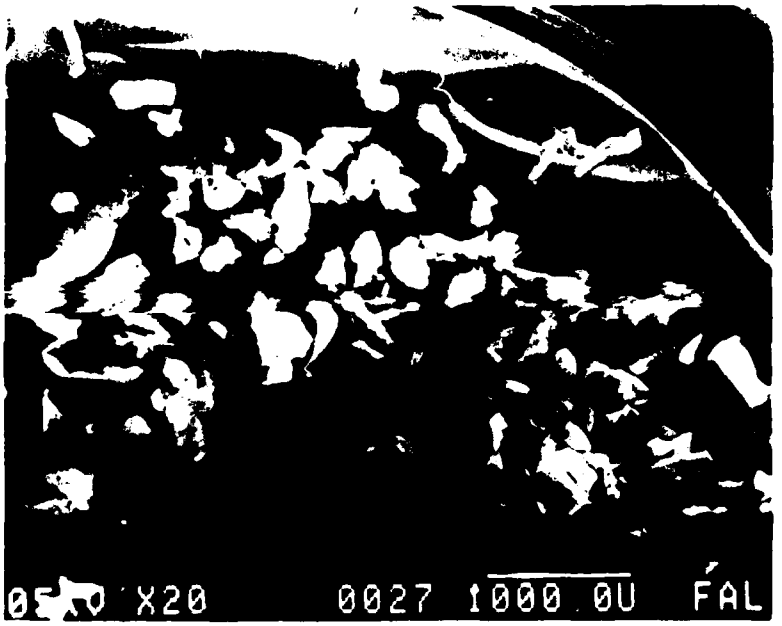


Figure 13. URQ (compare Figures 3 and 11). Room temperature and 18 hours elapsed time for Figures 13-17 (see text).

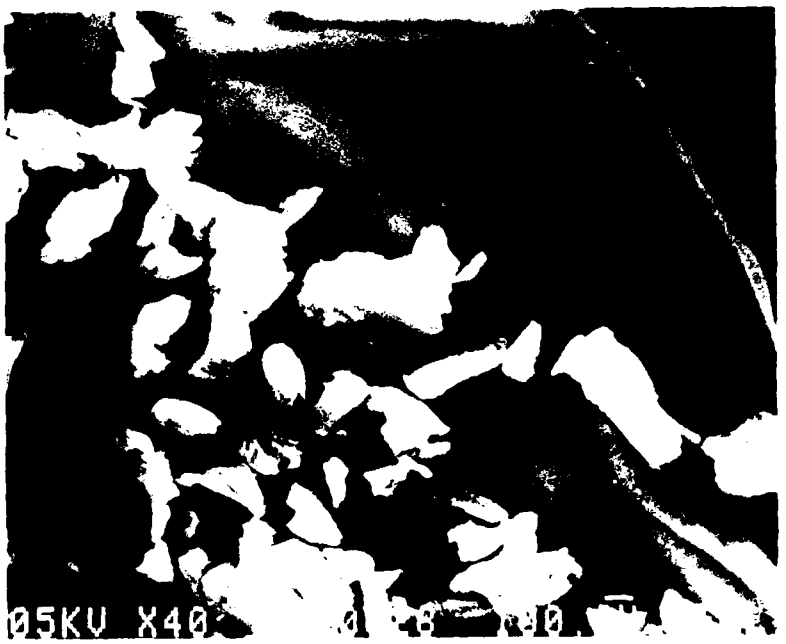


Figure 14. Detail in the URQ, Including the Absence of Beam Damage (compare Figures 7 and 11).


Figure 15. Detail in the URQ.

Figure 16. Surface Regularization (compare Figures 8 and 9).


Figure 17. Beam Damage Rectangle Formed by 25 kV Electron Beam.

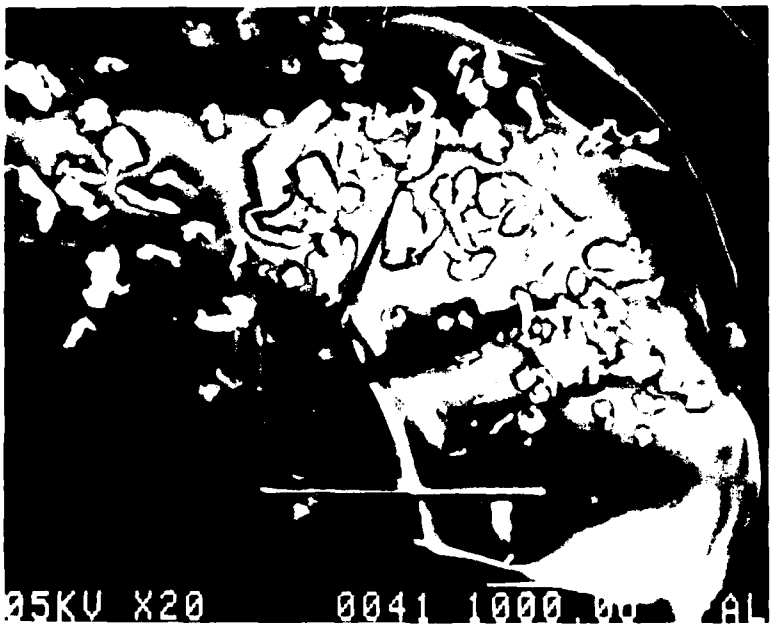


Figure 18. URQ (compare Figure 13).


Figure 19. Particle P#2 (compare Figures 14 and 15).


Figure 20. Particle P#2 (compare Figures 14 and 15).

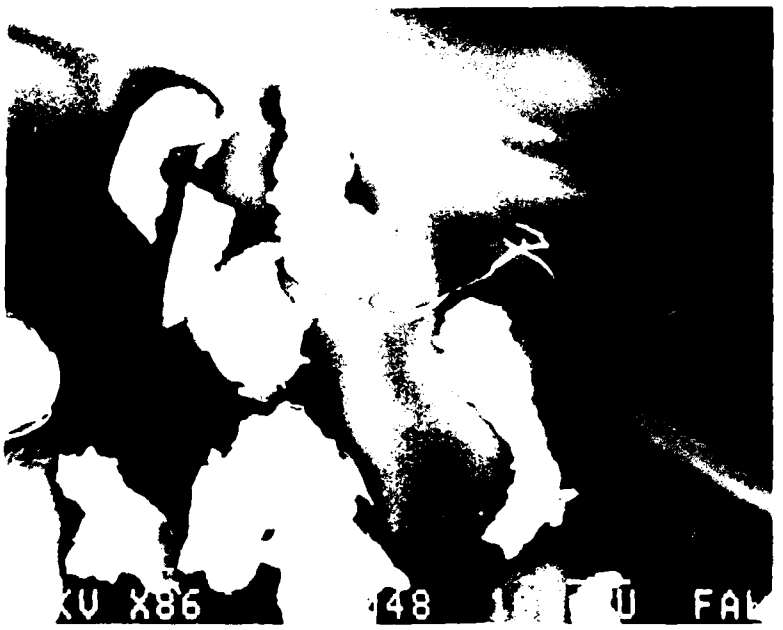


Figure 21. Crack Size Relative to Figure 16.

Figure 4 shows P #1 at higher magnification. It is not certain if the dark rings around the metal particles are shadows or indentations formed when the metal particles were originally arranged on the surface by micro-duster air pressure.

Apparent visibility differences can arise from picture to picture in the SEM, but much of the fine detail of the polymer surface roughness was seen to be reproducible. Figure 5 shows P #2 in the center as well as the adjacent end slit of one pie cut. Notice, for reference below, a small particle adjacent to one end of P #2. Figure 6 shows the junction between pie cut and slit shown near the center of Figure 5. Figure 7 is essentially a repeat of Figure 5, showing the electron-beam effect of Figure 6 (rectangular region).

A long fiber, defined as P #3, is shown in Figures 8-9 in the general location indicated on Figure 3. Again, the metal particles may or may not be indented into the surface. At any rate, they are held firmly, as determined immediately after sprinkling the surface by tapping into the cylinder on its side. Figure 10 shows some detail of the LRQ, including some electron beam damage.

After 4 hours at -135°C, Figure 11 (URQ) was obtained and should be compared to Figure 3. There appears to have been some polymer smoothing near the upper center of Figure 11, but not on the left hand side (possibly due to a visibility variation). Two rectangular beam-damage areas persist on the far right center of Figure 11, due to beam damage from Figure 6. Figure 12 shows that damage more clearly. A photomicrograph of P #1 (not shown) shows no essential change from the condition of Figure 4.

After the warm-up period to room temperature, Figure 13 shows the URQ corresponding to Figures 3 and 11. Now there has been a definite polymer surface leveling effect. Some charging is seen as a horizontal band. Notice the vicinity of P #2:

(i) The cut width has been reduced.

(ii) P #2 is no longer over the cut.

(iii) The small particle near the end of P #2 has "changed sides," i.e., moved relative to P #2. This shows that some chains are firmly attached to the particle and have translated it across the surface as chain mobility allows relief of internal stress and healing of the slice interface.

Figures 14 and 15 show the foregoing observations in more detail, in addition to the absence of the previous beam-damaged rectangles (Figures 7 and 11). Compare especially Figures 5 and 15. Particle P #1 appears similar to Figure 4. Figure 16 (P #3) compares to Figures 8-9 and again shows surface regularization and crack healing. Figure 17 shows a 25 kV beam-damage rectangle created just before the sample was taken out for annealing.

After the annealing treatment, the smooth polymer surface was generally preserved, as in Figure 18. However, some additional pucker ridges can be seen to have formed due to the thermal treatment. Figures 19 and 20, compared to Figures 14 and 15 show a somewhat more healed slit region near P #2. Figure 21 shows some crack size reduction relative to Figure 16 (zipper effect starting at the nearby continuous edge). However, the great change in particle positions, in this case, could conceivably have been caused by the annealing operation outside the SEM. It should also be noted that annealing reduced the 25 kV beam-damage rectangle seen in Figure 17 to the level seen in Figure 18.

## IV. DISCUSSION AND CONCLUSIONS

Since the mechanically damaged surface was created at room temperature and then cooled, it cannot be proven what fraction of the surface features is mechanically induced and what fraction is thermally induced. No matter how formed, however, many of the irregularities persist after several hours at -135°C, which is still somewhat above $T_g$. After heating to room temperature, the disappearance of some features such as pucker lines could be attributed to bulk volume changes, but the dramatic surface smoothing can surely be interpreted as due to a surface rearrangement of chains, consistent with a bulk melting effect in RTV-142 near -40°C.

In the beam-damaged areas the local effective temperature must have been fairly high (considerably above room temperature) in order to form the rectangular raised regions. There was no appreciable surface chain mobility available during 4 hours at -135°C, near $T_g$ (Figure 12). However, room temperature annealing (on the order of 10 hours) allowed sufficient chain mobility for smoothing (Figure 14). Of course an extremely high-energy electron beam (25 kV instead of 5 kV) may cause enough polymer degradation that complete healing becomes impossible, even after 100°C annealing (Figures 17 and 18).

The observed crack healing (e.g., in Figure 15 compared to Figure 5) could, again, in principle be attributed to a bulk effect in mating two surfaces. However, this is also consistent with the results of extensive research on crack healing in polymers,[15] which describes not only surface contact and wetting, but also interdiffusion of chains from each side into the other.

The variation of surface features observed with the SEM is consistent with the pore-penetration equation, Eq. (1), which states that 99% of 100 Å pores are filled by a material possessing a surface energy on the order of $10^2$ erg/cm$^2$. We performed three complementary calculations of the surface energy of an idealized amorphous solid polymer and conducted detailed SEM investigations leading to the following conclusions:

1. The first surface-energy calculation, from the conformational energy theory of chain folding, gave a lesser order of magnitude (16 erg/cm$^2$) using the available information on energy per fold.

2. The last two calculations, which considered different ways of estimating the entropy decrease and free energy increase caused by deformed Gaussian coils near a free surface, did give $\sigma \approx 300$ to 400 erg/cm$^2$.

3. Therefore, entropically driven pore penetration and adhesion is theoretically expected for ideal amorphous polymer systems.

4. The observed time- and temperature-dependence of the cut widths and surface features, as well as the motion of particle P #2 and the filleting and vortex formation in Figures 1 and 2, are consistent with temperature-dependent surface chain mobility in RTV-142. This is consistent with the flow of polymer chain segments around foreign particle asperities, i.e., adhesion.

## REFERENCES


1. D. J. Alner, ed., Aspects of Adhesion-2, University of London Press (1964).

2. C. Kittel, Introduction to Solid State Physics, 5th ed., John Wiley, 1976 (p.78).

3. J. N. Anand, J. of Adhesion, 1, 31 (1969).

4. D. H. Buckey, Metal-Dielectric Interactions, NASA Technical Memorandum 79151, prepared for the Conference on Electrical Insulation and Dielectric Phenomena sponsored by the National Research Council, Whitehaven, PA, October 21-25, 1979.

5. N. J. DeLollis, Adhesion Theory Review and Critique, Sandia Laboratories, SC-RR-70-915, December 1970.

6. D. E. Packham, "The Adhesion of Polymers to Metals: The Role of Surface Topography," in K. L. Mittal, ed., Adhesion Aspects of Polymeric Coatings, Plenum, NY (1983).

7. R. P. Wool, ACS Preprints (PMSE), Vol. 51, p. 179 (1984).

8. F. Reif, Statistical Physics, McGraw-Hill, NY (1965).

9. E. A. DiMarzio, J. Chem. Phys. 42, 2101 (1965).

10. K. F. Freed, Adv. Phys. Chem. 22, 1 (1972).

11. H. Tadokoro, Structure of Crystalline Polymers, John Wiley, New York (1979), p.137.

12. T. W. Husby, H. O. Bair, and R. Salovey, ACS Preprints, 9, 795 (1968).

13. Illers and Hendus, Makromol. Chemie, 113, 1 (1968).

14. J. D. Hoffman, Davis, and J. I. Lauritsen, Jr., Ch. 7 in B. Hannay, ed., Treatise on Solid State Chem., pp.529-538.

15. R. P. Wool and K. M. O'Connor, J. Appl. Phys., 52, 5953 (1981). Y. W. Kim and R. P. Wool, Macromolecules, 16, 1115 (1983). R. P. Wool, Rubber Chem. and Tech., 57 (2), 307 (1984).

## LABORATORY OPERATIONS

The Laboratory Operations of The Aerospace Corporation is conducting experimental and theoretical investigations necessary for the evaluation and application of scientific advances to new military space systems. Versatility and flexibility have been developed to a high degree by the laboratory personnel in dealing with the many problems encountered in the nation's rapidly developing space systems. Expertise in the latest scientific developments is vital to the accomplishment of tasks related to these problems. The laboratories that contribute to this research are:

Aerophysics Laboratory: Launch vehicle and reentry fluid mechanics, heat transfer and flight dynamics; chemical and electric propulsion, propellant chemistry, environmental hazards, trace detection; spacecraft structural mechanics, contamination, thermal and structural control; high temperature thermomechanics, gas kinetics and radiation; cw and pulsed laser development including chemical kinetics, spectroscopy, optical resonators, beam control, atmospheric propagation, laser effects and countermeasures.

Chemistry and Physics Laboratory: Atmospheric chemical reactions, atmospheric optics, light scattering, state-specific chemical reactions and radiation transport in rocket plumes, applied laser spectroscopy, laser chemistry, laser optoelectronics, solar cell physics, battery electrochemistry, space vacuum and radiation effects on materials, lubrication and surface phenomena, thermionic emission, photosensitive materials and detectors, atomic frequency standards, and environmental chemistry.

Computer Science Laboratory: Program verification, program translation, performance-sensitive system design, distributed architectures for spaceborne computers, fault-tolerant computer systems, artificial intelligence and microelectronics applications.

Electronics Research Laboratory: Microelectronics, GaAs low noise and power devices, semiconductor lasers, electromagnetic and optical propagation phenomena, quantum electronics, laser communications, lidar, and electro-optics; communication sciences, applied electronics, semiconductor crystal and device physics, radiometric imaging; millimeter wave, microwave technology, and RF systems research.

Materials Sciences Laboratory: Development of new materials: metal matrix composites, polymers, and new forms of carbon; nondestructive evaluation, component failure analysis and reliability; fracture mechanics and stress corrosion; analysis and evaluation of materials at cryogenic and elevated temperatures as well as in space and enemy-induced environments.

Space Sciences Laboratory: Magnetospheric, auroral and cosmic ray physics, wave-particle interactions, magnetospheric plasma waves; atmospheric and ionospheric physics, density and composition of the upper atmosphere, remote sensing using atmospheric radiation; solar physics, infrared astronomy, infrared signature analysis; effects of solar activity, magnetic storms and nuclear explosions on the earth's atmosphere, ionosphere and magnetosphere; effects of electromagnetic and particulate radiations on space systems; space instrumentation.

END

FILMED

3-86

DTIC